

# Single-pixel edge enhancement of object via convolutional filtering with localized vortex phase

JIGME ZANGPO\* AND HIROKAZU KOBAYASHI.

*Graduate School of Engineering, Kochi University of Technology, 185 Miyanokuchi, Tosayamada, Kami City, Kochi 782-8502, Japan*

*\*jigmezangpo11@gmail.com*

**Abstract:** Microscopy is an essential tool in imaging research, and the edge-enhanced microscope by using the vortex filter is of particular interest as an optical information processing that highlights amplitude and phase edges of object in all directions. The application of this technique is not limited to the visible range, but edge enhancement of object in invisible wavelength is also crucial for near-infrared fluorescence and electronic circuit inspection through silicon semiconductors. One disadvantage of near-infrared imaging is that digital cameras such as CCD and CMOS become much more expensive than cameras for the visible spectrum. As an cost-effective method to implement invisible edge enhancement, the Fourier single-pixel imaging has already been proposed without using a camera, but using a single-pixel detector. However, this method requires 3 or 4 times more single-pixel measurements due to the three-phase or four-phase shift to detect optical complex amplitude in Fourier domain. In response, we propose a method for single-pixel edge enhancement of object via convolutional filtering with a localized vortex phase, eliminating the extra single-pixel measurements required by the phase-shifting method. Our simulation results show that the correlation coefficient between the ideal edges of an object and the edge enhanced by our proposed method is 0.95, indicating that our method is effective way to detect the edges. This novel and effective approach for enhancing and detecting the edges of object can be valuable in various invisible imaging applications.

© 2024 Optica Publishing Group

## 1. Introduction

Microscopy is an essential tool in imaging research, and edge-enhanced microscope with a vortex filter has been particularly attracted more attention to enhance the edges of phase and amplitude objects due to their capability for all-directional edge enhancement [1–6], while differential interference-contrast microscopy enhances edges in only one-direction [7]. The application of this technique is not limited to the visible range, but edge enhancement of object in invisible wavelength is also crucial for near-infrared fluorescence and electronic circuit inspection through silicon semiconductors. One disadvantage of near-infrared imaging is that digital cameras, such as silicon-based charge-coupled devices (CCD) and complementary metal-oxide-semiconductors (CMOS), tend to become expensive than cameras for the visible spectrum [8].

To address this issue, researchers have opted for a more cost-effective approach by utilizing single-pixel detectors with reconstruction of two-dimensional image by correlation calculation [8–10]. The so-called single-pixel imaging can detect the weak signal and image with a high speed [11–14]. In Refs. [15–17], researchers used single-pixel imaging to capture complex amplitude distribution of objects using a four-step phase-shifting technique. Subsequently, researchers attempted to integrate single-pixel imaging into an edge-enhanced microscope, where Fourier single-pixel imaging was adopted to capture the edges of the phase object using four or three-step phase shifting [18–21]. The advantage of their approach is the absence of a vortex filter, instead, they utilized a digital micromirror device (DMD) to generate a reference wave

and an optical vortex with the assistance of a super-pixel technique [22–24], which is highly robust and easy to use while offering full spatial control over the phase and amplitude of a light field [22, 25]. While this method successfully detected and enhanced the edges of the phase object, the drawback is that due to the four or three-step phase shifting, resulting in four or three times single-pixel measurements are required for reconstruction.

To reduce the number of single-pixel measurements, we propose a method, namely, a single-pixel edge-enhanced microscope via convolutional filtering with a localized vortex phase, which can eliminate the extra single-pixel measurements required by the phase-shifting method. We conducted numerical simulations to validate this approach, resulting in that the correlation coefficient of edge enhancement of the object through our proposed method and ideal edge enhancement is 0.95, which indicates that the proposed method is indeed capable of effectively enhancing the edges of object.

In Section 2 we describe proposed method, the single-pixel edge enhancement of object, and principle of super-pixel method. In Sections 3, we present the numerical simulation results. Section 4 concludes the study.

## 2. Single-pixel Edge Enhancement via Convolutional Filtering with Localized Vortex Phase

### 2.1. Principle of single-pixel edge enhancement via convolutional filtering

Figure 1 shows  $4f$  system with a vortex filter to implement all-directional edge enhancement placed after the bright-field microscope. The  $4f$  system consists of object plane, Fourier plane and image plane. At the object plane, the object magnified by the bright-field microscope is a phase-amplitude object (PAO), whose brightness (from 0 to 1) denotes amplitude and color denotes phase. In the object, a yellow circle and a horizontal black strip indicate a phase object and an amplitude object, respectively. The input object  $f_{in}(\mathbf{r})$  magnified by the bright-field microscope undergoes the Fourier transformation by first lens and the Fourier spectrum is given by  $F(\mathbf{k}) = \mathcal{F}\{f(\mathbf{r})\}$ , where  $\mathcal{F}$  represents the Fourier transform and  $\mathbf{k} = (k_x, k_y)$  denotes the two-dimensional transverse wavenumber vector. Then,  $F(\mathbf{k})$  is modulated by vortex phase plate,  $H(\mathbf{k}) = e^{i\theta}$  with an azimuthal angle  $\theta$  at the Fourier plane and the image is obtained after inverse Fourier transform by second lens as follow:

$$f_{out}(\mathbf{r}) = \mathcal{F}^{-1}\{F(\mathbf{k})H(\mathbf{k})\} = f_{in}(\mathbf{r}) * h(\mathbf{r}), \quad (1)$$

where  $*$  denotes the convolution and  $h(\mathbf{r}) = \frac{i}{2\pi} \frac{e^{i\theta}}{r^2}$  is the inverse Fourier transform of  $H(\mathbf{k})$  and denotes the point spread function of the optical system with a vortex phase plate as the Fourier filter. The PAO, captured by the bright-field microscope, undergoes edge enhancement by the  $4f$  system in Fig. 1, as shown at image plane.

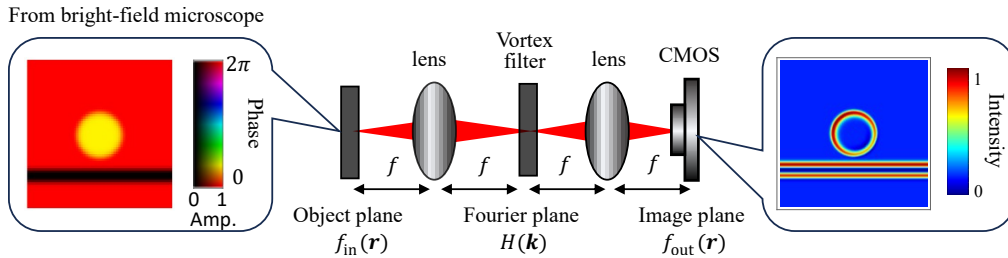


Fig. 1. The  $4f$  system with a vortex filter for all-directional edge enhancement..

In Eq. (1),  $h(\mathbf{r}) = \frac{i}{2\pi} \frac{e^{i\theta}}{r^2}$  consists of a spiral phase  $e^{i\theta}$  and a localized amplitude function  $a(\mathbf{r}) \propto 1/r^2$ . In general, requirement of the filter function for the edge enhancement is the

localized amplitude function multiplied with the azimuthal phase, i.e.,  $h(\mathbf{r}) = a(\mathbf{r})e^{i\theta}$ . The convolution of  $f_{\text{in}}(\mathbf{r}) * h(\mathbf{r})$  can be rewritten as

$$f_{\text{out}}(\mathbf{r}) = \iint_{-\infty}^{\infty} f_{\text{in}}(\mathbf{r}')h(\mathbf{r} - \mathbf{r}')d\mathbf{r}' = \mathcal{F}\{f_{\text{in}}(\mathbf{r}')h(\mathbf{r} - \mathbf{r}')\}(0), \quad (2)$$

where the object  $f_{\text{in}}(\mathbf{r})$  multiplies with shifted patterns of  $h(\mathbf{r})$  and then Fourier transformed, followed by extracting the center amplitude. Equation (2) can be implemented as shown in Fig. 2, where the object light is multiplied with the shifted localized vortex phase  $h(\mathbf{r} - \mathbf{r}')$  generated by the super-pixel method using the DMD and then Fourier transformed by Fourier lens in the  $2f$  system, followed by extracting the desired location with an aperture. This aperture has two functions: the first function is to select the first-order diffraction to generate the localized vortex phase by super-pixel method as shown later; the second function is to select the center position according to Eq. (2). Finally, the single-pixel detector, such as photodiode, measures the corresponding optical power for different patterns over time to reconstruct the enhanced edges of the object by reshaping one-dimensional temporal data to two-dimensional format, as shown in Fig. 2 with the caption 'Edge Enhancement'.

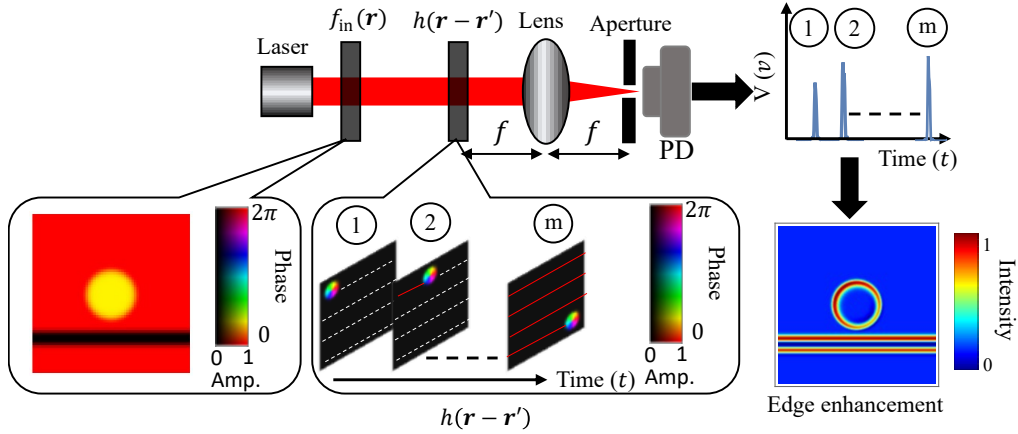


Fig. 2. Single-pixel edge-enhanced microscope via convolutional filtering. In  $m$  different patterns, a white dot denotes the scanning path of patterns, while a red line denotes the patterns that have completed the scanning. For each scanning of pattern, the photodiode measures the corresponding optical power as voltage data in time and the edge-enhanced image can be obtained by reshaping the temporal voltage data to two-dimensional format.

## 2.2. Generation of localized vortex phase by super-pixel method with DMD

Unlike a spatial light modulator (SLM), which can generate phase and amplitude holograms [26–30], the DMD can only generate binary amplitude hologram represented by binary reflections with 1 or 0 indicating turn on and off, respectively. In the super-pixel method [25], however, both the amplitude and phase modulation of light wave can be implemented by extracting the first-order diffraction generated by the binary amplitude hologram. This method offers higher beam shaping fidelity than SLMs [31] and much faster refresh rates over 10 kHz for binary amplitude patterns, whereas most SLMs are limited to 120 Hz [32]. However, these advantages come at the expense of limited modulation depth and low diffraction efficiency [31].

Figure 3 (a) shows schematic  $4f$  setup of the super-pixel method to obtain full spatial control over the phase and amplitude of light on target plane [22]. The DMD placed at the front focal

plane of the first lens is partitioned into super-pixels, which are square sub-groups of  $n \times n$  micromirrors. The diffracted light from the DMD is Fourier transformed by the first lens and an aperture with radius of  $R$  acts as a spatial filter on the Fourier plane to capture the first-order diffraction. The position of the aperture is selected to ensure that the responses of adjacent pixels within the super-pixel on the DMD exhibit a phase difference of  $2\pi/n^2$  in the  $x$ -direction and  $2\pi/n$  in the  $y$ -direction, as shown in Fig. 3 (b), where some pixels are highlighted with green color to indicate that they are turned on. Figure 3 (c) shows the appropriate aperture position, which is obtained as  $(x, y) = (-\rho, n\rho)$ , where  $\rho = \frac{-\lambda f}{n^2 d}$ ,  $\lambda$  is the wavelength of the light,  $f$  is the focal length of the first lens and  $d$  is pixel size of the micromirror. Here we notice that optimizing the aperture radius  $R$  is crucial because a small  $R$  will reduce the desired signal and a large  $R$  will contain the undesired zero-order diffraction. The first-order diffraction extracted by the aperture further undergoes inverse Fourier transform by the second lens and the resultant  $E_{\text{out}}$  at the target plane is proportional to the sum of only valid phases on individual pixel responses, which are evenly distributed on the complex plane along a circle as shown in Fig. 3 (d). To determine the resultant of electric field  $E_{\text{out}}$  at the target plane, we used the following equation:

$$E_{\text{out}} = E_{\text{in}} \sum_{m=0}^{n^2-1} D_m e^{i2\pi m/n^2}, \quad (3)$$

where  $E_{\text{in}}$ ,  $D_m$  and  $n$  denote the input electric field, the binary values 0 or 1 of the  $m$ -th pixel within the super-pixel, and the super-pixel size, respectively. As shown in Fig. 2, the second  $2f$  system in Fig. 3 (a) is not required in the proposed single-pixel edge enhancement, due to the Fourier transform in Eq. (2).

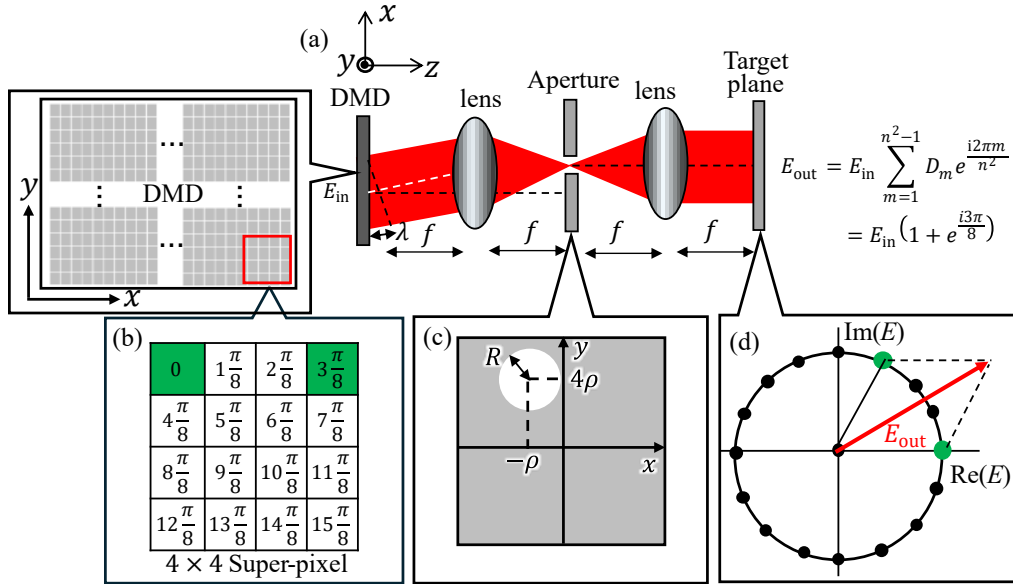


Fig. 3. (a) Setup of super-pixel method. (b) Super-pixel with the size of  $4 \times 4$  pixels exhibiting a phase difference of  $2\pi/n^2$  in the  $x$ -direction and  $2\pi/n$  in the  $y$ -direction. Two pixels with green color are turned on with 100% reflectance while the other pixels are turned off with 0% reflectance. (c) Aperture with radius of  $R$  placed at  $(-\rho, 4\rho)$  on the Fourier plane to extract the first-order diffraction of DMD. (d) The resultant field  $E_{\text{out}}$  (red arrow) on the target plane is proportional to the sum of the phases on the pixels that are turned on.

In Fig. 4 (a), we plot the complex amplitude for all possible combinations of  $D_m$  within the super-pixel with the size of  $n = 4$ . As can be seen from Fig. 4 (a), the possible complex amplitude is distributed within a disk with radius of  $\cot(\pi/n^2) \approx 5$  on the complex plane. In the set of 65536 patterns, there are many duplicated complex fields and only 6561 patterns have unique fields. For the purpose of making a hologram using the super-pixel method, each pixel in the desired complex function is replaced with an appropriate super-pixel with the size of  $n \times n$ . The replacement process involves comparing the resultant field of the super-pixel with each pixel in the desired complex function and the nearest values from all the possible fields generated by the super-pixel are then assigned to each pixel in the desired complex function. Figure 4 (b) illustrates a grid of  $16 \times 16$  pixels of the desired function with localized vortex phase. By employing the super-pixel method, each  $4 \times 4$  super-pixel replaces individual pixels in the desired complex function in Fig. 4 (b), resulting in a hologram pattern as shown in Fig. 4 (c) with a dimension of  $64 \times 64$  pixels.

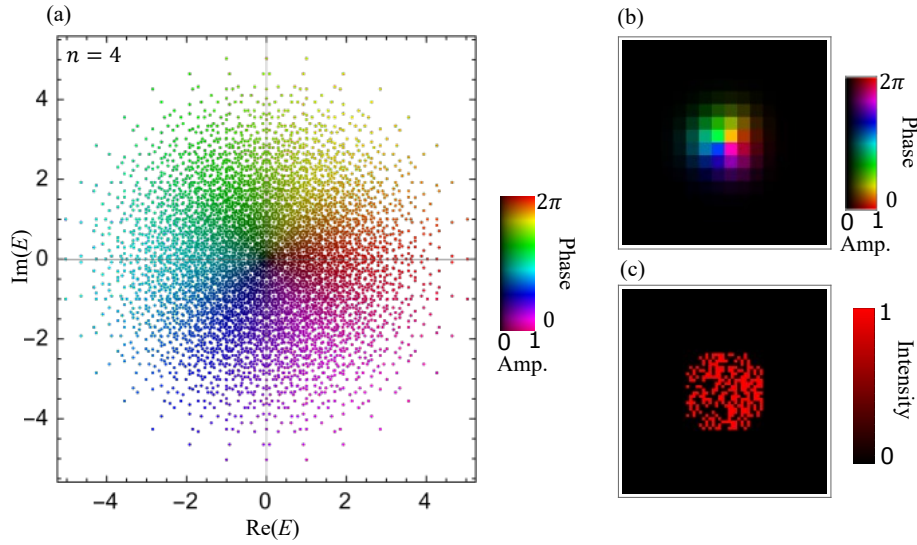


Fig. 4. (a) Complex amplitude generated by all possible combinations of pixels corresponding to the super-pixel with  $n = 4$ . (b) The desired complex amplitude distribution with  $16 \times 16$  pixels. (c) The hologram with  $64 \times 64$  pixels generated by replacing super-pixel  $4 \times 4$  to the  $16 \times 16$  desired complex function.

### 3. Numerical Simulation Results of the Proposed Method

#### 3.1. Edge enhancement capability of localized amplitude functions

In this section, we consider several types of the localized amplitude functions  $a(\mathbf{r})$ , such as  $\frac{1}{r^2}$ ,  $\frac{1}{r}$ ,  $\frac{1}{\sqrt{r}}$  and  $e^{-r^2/w^2}$  with the radius  $w$ , as plotted in Fig. 5 (a), where we used the optimized radius  $w = 35 \mu\text{m}$  for the Gaussian function, explained in Section 3.3. The complex amplitude distribution of  $h(\mathbf{r}) = a(\mathbf{r})e^{i\theta}$  with the several localized amplitude functions  $a(\mathbf{r})$  are shown in Figs. 5 (b) - (e). Here we note that  $\frac{1}{r^2}$ ,  $\frac{1}{r}$ , and  $\frac{1}{\sqrt{r}}$  in Fig. 5 are normalized by their function values at  $r_{\min}$ , which is the minimum radial value in the simulation coordinate.

Before using the super-pixel method, we used Eq. (1) to numerically verify the edge enhancement capability of the localized amplitude functions. Here we consider the PAO in Fig. 6 (a) as the object. We first perform inverse Fourier transform on  $h(\mathbf{r})$  to obtain  $H(\mathbf{k})$  and then perform a Fourier transform on the PAO, followed by multiplication with  $H(\mathbf{k})$ . Finally, we

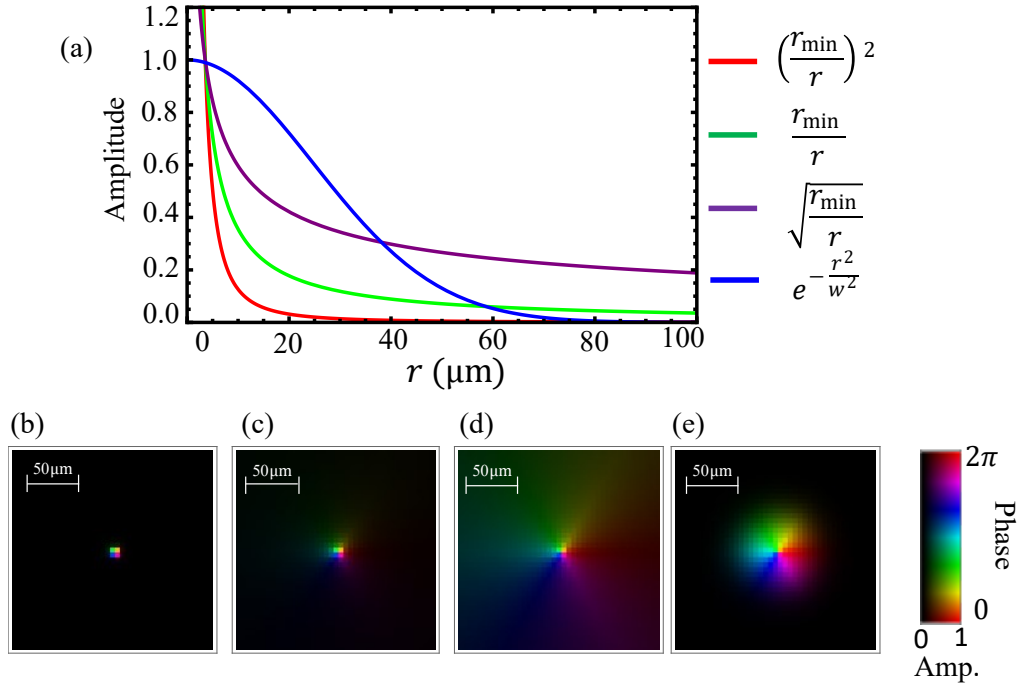


Fig. 5. (a) Radial dependence of the amplitude functions,  $\frac{1}{r^2}$ ,  $\frac{1}{r}$ ,  $\frac{1}{\sqrt{r}}$  and  $e^{-r^2/w^2}$  with  $w = 35 \mu\text{m}$ . (b-e) Corresponding complex amplitude distributions of the localized vortex phase.

apply an inverse Fourier transform to the Fourier spectrum and then take the absolute square to obtain the edges of the PAO. The simulation parameters are as follows: a wavelength of 635 nm, a total dimension of  $1\text{mm} \times 1\text{mm}$ , a step size of  $1/199\text{mm} \times 1/199\text{mm}$ , which corresponds to  $200 \times 200$  pixels.

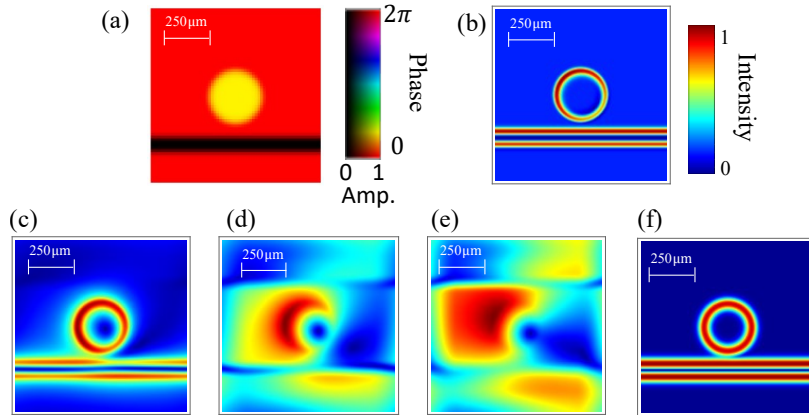


Fig. 6. Edge enhancement capability of several localized amplitude functions. (a) Complex amplitude distribution of the PAO. (b) Ideal edge enhancement. (c-f) Edge enhancement using  $\frac{1}{r^2}$ ,  $\frac{1}{r}$ ,  $\frac{1}{\sqrt{r}}$ , and  $e^{-r^2/w^2}$  with  $w = 35 \mu\text{m}$  in  $h(r)$ , respectively.

Figure 6 shows the numerical simulation results of the edge enhancement using the localized

vortex phase  $h(\mathbf{r})$ . Figure 6 (b) shows the ideal edge enhancement of PAO by using  $H(\mathbf{k}) = k_r e^{i\theta}$  with  $k_r \equiv \sqrt{k_x^2 + k_y^2}$ , while Figs. 6 (c-f) illustrate edge enhancement using the localized amplitude functions  $a(r)$ . The localized amplitude functions  $\frac{1}{r}$  and  $\frac{1}{\sqrt{r}}$  failed to detect the edges of the PAO while the functions  $\frac{1}{r^2}$  and  $e^{-r^2/w^2}$  successfully detected the edges of the PAO. The correlation coefficients between ideal edge enhancement in Fig. 6 (b) and Figs. 6 (c-f) are 0.80, 0.25, 0.06 and 0.85, respectively. The reason why the amplitude functions  $\frac{1}{r}$  and  $\frac{1}{\sqrt{r}}$  of optical vortex failed to detect the edges of object is that their radial dependence is not tightly localized compared to  $\frac{1}{r^2}$  and  $e^{-r^2/w^2}$ , i.e., the tails of the radial dependence for the amplitude functions  $\frac{1}{r}$  and  $\frac{1}{\sqrt{r}}$  do not rapidly approach to zero, instead, they exhibit higher value, as can be seen in Fig. 5 (a).

### 3.2. Fidelity estimation of super-pixel method to generate localized vortex phase

The modulation accuracy of the super-pixel method between the target field  $E_{\text{out}}$  and the desired field  $E_{\text{desire}}$  can be quantified by calculating their fidelity  $F$  as shown below:

$$F = \frac{|E_{\text{desire}}^* \cdot E_{\text{out}}|^2}{|E_{\text{desire}}|^2 |E_{\text{out}}|^2}, \quad (4)$$

where the two-dimensional distributions  $E_{\text{out}}$  and  $E_{\text{desire}}$  are reshaped into one column and their inner product is calculated in the numerator, and  $*$  denotes the complex conjugate.  $F = 1$  indicates that the target fields and the desired fields are the same, whereas  $F = 0$  means they are completely different.

We conducted a numerical simulation to estimate the fidelity between the target field generated by the super-pixel method and the desired localized vortex phase with the amplitude functions,  $(c/r)^2$ ,  $c/r$ ,  $\sqrt{c/r}$  and  $ce^{-r^2/w^2}$ , where  $c$  denotes amplitude coefficient. The optimizing parameters to obtain the best fidelity in the super-pixel method are the amplitude coefficient  $c$  and the aperture radius  $R$ . For the Gaussian amplitude function, an additional parameter  $w$  needs to be optimized and here we used  $w = 100 \mu\text{m}$ , which gives the highest fidelity of 0.89. The simulation conditions remain the same as those in Section 3.1, with an additional parameter, a focal length of the lens setting at 300 mm.

Figures 7 (a-d) show the simulation results of the fidelity between the ideal and the generated localized vortex phases with different  $a(r)$ :  $(c/r)^2$ ,  $c/r$ ,  $\sqrt{c/r}$  and  $ce^{-r^2/w^2}$ , respectively. The horizontal and vertical axes in Fig. 7 show the aperture radius  $R$  normalized by aperture position  $\rho$  and the amplitude coefficient  $c$  of  $h(\mathbf{r})$ , respectively. Table 1 shows summary of the maximum fidelities and the corresponding optimized parameters. The Gaussian amplitude function  $e^{-r^2/w^2}$  provides fidelity 0.89, whereas  $\frac{1}{r^2}$ ,  $\frac{1}{r}$  and  $\frac{1}{\sqrt{r}}$  yield fidelity values below 0.6 (refer to Table 1), because these power functions increase rapidly as they approach to the origin, resulting in low fidelity with the finite amplitudes in the super-pixel method. Even if the fidelity to the desired function is low, however, edge enhancement might be possible if a certain degree of localization is achieved by the amplitude function. Thus, in the next section, we use the amplitude functions  $\frac{1}{r^2}$  and  $e^{-r^2/w^2}$  which successfully performed edge enhancement in Fig. 6, to evaluate our single-pixel method via convolutional filtering.

### 3.3. Edge enhancement capability of single-pixel imaging via convolutional filtering with localized vortex phase

Now, we evaluate edge enhancement capability of our proposed single-pixel imaging method with the localized amplitude functions,  $\frac{1}{r^2}$  and  $e^{-r^2/w^2}$ . We first prepared the binary hologram on the DMD to generate the shifted localized vortex phase  $h(\mathbf{r}' - \mathbf{r})$  by using the super-pixel method with  $n = 4$ . By following the principles of Section 2.1, we calculated Fourier transform of the object light multiplied with the hologram on the DMD and then obtained optical power

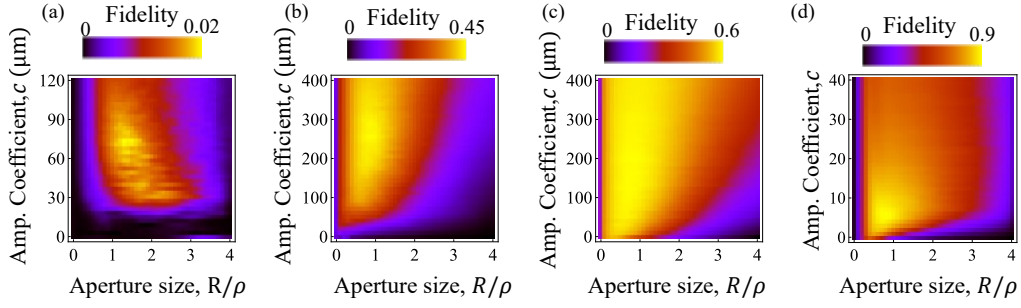


Fig. 7. (a-d) The fidelity of localized vortex phase with amplitude functions:  $\frac{1}{r^2}$ ,  $\frac{1}{r}$ ,  $\frac{1}{\sqrt{r}}$  and  $e^{-r^2/w^2}$  ( $w = 100 \mu\text{m}$ ) for different amplitude coefficients  $c$  and aperture radius,  $R$  normalized by aperture position  $\rho$ .

Table 1. Simulation results of maximum fidelity and optimized parameters with different  $a(r)$

Parameter	$a(r)$	$\frac{1}{r^2}$	$\frac{1}{r}$	$\frac{1}{\sqrt{r}}$	$e^{-r^2/w^2}$
Max. fidelity, $F$		0.02	0.45	0.57	0.89
Radius, $R/\rho$		2.5	2.6	2	0.7
Amp. coefficient, $c$		42 $\mu\text{m}$	100 $\mu\text{m}$	100 $\mu\text{m}$	9

at the center point of the aperture,  $(x, y) = (-\rho, n\rho)$ , to reconstruct the two-dimensional edge enhanced image. The simulation conditions remain the same as those in Section 3.1.

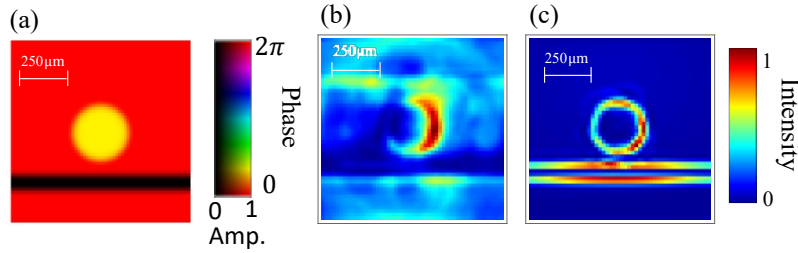


Fig. 8. (a) Distribution of PAO, (b) and (c) Edge enhancement via proposed method using optical vortex with the amplitude function  $1/r^2$  and  $e^{-r^2/w^2}$  with  $w = 35 \mu\text{m}$ , respectively.

Figure 8 (a) represent the complex amplitude distribution of the PAO. The ideal edge to compare with edge enhancement of the object by vortex phases with the amplitude function  $1/r^2$  and  $e^{-r^2/w^2}$  is same as Figs. 6 (c) and (d) but with a different pixel size i.e.,  $50 \times 50$ , which represents the total pixel size for the single-pixel edge enhancement reconstruction. The best edge enhancement using localized vortex phases with the amplitude function  $1/r^2$  and  $e^{-r^2/w^2}$  are shown in Figs. 8 (b) and (c), respectively. The amplitude function  $e^{-r^2/w^2}$  could successfully enhance the edge of the object using the proposed single-pixel edge enhancement technique while the amplitude function  $1/r^2$ , which could successfully enhance the edge in Section 3.1, failed to



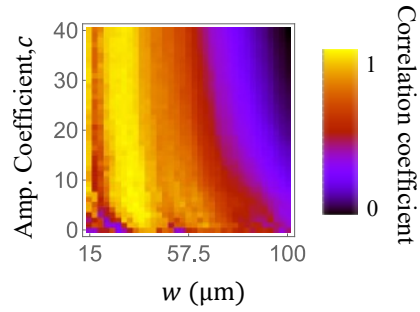


Fig. 9. Correlation coefficient between the edge enhanced by the Gaussian amplitude function of the optical vortex and the ideal edge enhancement for varying values of  $w$  and amplitude coefficient  $c$ .

enhance the edge. The main reason of this failure is considered as low fidelity (0.02), as shown in Table 1. Figure 9 shows dependence of the correlation coefficient between the single-pixel edge enhancement by using the Gaussian amplitude function and the ideal edge enhancement on the optimizing parameters  $w$  and  $c$ . We selected the starting point of  $w$  greater than  $15\ \mu\text{m}$ , which exceeds the radius of the super-pixel size of  $10\ \mu\text{m}$ , because  $w$  values lower than  $15\ \mu\text{m}$  do not detect the edges of the object. The highest correlation coefficient 0.95 is achieved when  $w = 35\ \mu\text{m}$  and  $c = 6$ . The edge enhancement using these optimized parameters is illustrated in Fig. 8 (c). The strong and positive relationship between the ideal edge and the proposed method's edge demonstrates that the proposed approach is indeed capable of effectively enhancing the edges of objects.

#### 4. Conclusion

In this paper, we proposed and numerically demonstrated edge enhancement of objects using single-pixel imaging via convolutional filtering, in which the localized vortex phase consists of a spiral phase  $e^{i\theta}$  and a localized amplitude function  $a(r)$ . We have tested several localized functions to find the highest fidelity using super-pixel method for use in our proposed method and a Gaussian amplitude function offers the highest fidelity (0.89). We numerically demonstrated the proposed method and the correlation coefficient between ideal edge enhancement and our method was 0.95. The results show that the proposed method is capable of enhancing the edge of the PAO while eliminating extra single-pixel measurements required by previous studies. Our proposed method would be applied to invisible wavelength range, such as near-infrared fluorescence and electronic circuit inspection through silicon semiconductor. We plan to conduct experimental demonstration of the proposed method in the future.

**Funding.** Japan Society for the Promotion of Science (18KK0079, 20K05364); Research Foundation for Opto-Science and Technology.

**Disclosures.** The authors declare no conflicts of interest.

**Data availability.** Data underlying the results presented in this paper are not publicly available at this time but may be obtained from the authors upon reasonable request.

#### References

1. S. Fürhapter, A. Jesacher, S. Bernet, and M. Ritsch-Marte, "Spiral phase contrast imaging in microscopy," *Opt. Express* **13**, 689–694 (2005).
2. A. Jesacher, S. Fürhapter, S. Bernet, and M. Ritsch-Marte, "Shadow effects in spiral phase contrast microscopy," *Phys. Rev. Lett.* **94**, 233902 (2005).
3. S. Bernet, A. Jesacher, S. Fürhapter, C. Maurer, and M. Ritsch-Marte, "Quantitative imaging of complex samples by spiral phase contrast microscopy," *Opt. Express* **14**, 3792–3805 (2006).

4. S. FÜRhapter, A. Jesacher, C. Maurer, S. Bernet, and M. Ritsch-Marte, "Spiral phase microscopy," *Adv. Imaging Electron Phys.* **146**, 1–59e (2007).
5. J. Zangpo, T. Kawabe, and H. Kobayashi, "Edge-enhanced microscopy of complex objects using scalar and vectorial vortex filtering," *Opt. Express* **31**, 38388–38399 (2023).
6. J. Zangpo and H. Kobayashi, "Isolation of phase edges using off-axis q-plate filters," arXiv preprint arXiv:2310.18044 (2023).
7. W. Lang, *Nomarski differential interference-contrast microscopy* (Carl Zeiss Oberkochen, 1982).
8. M. F. Duarte, M. A. Davenport, D. Takhar, J. N. Laska, T. Sun, K. F. Kelly, and R. G. Baraniuk, "Single-pixel imaging via compressive sampling," *IEEE Signal Process. Mag.* **25**, 83–91 (2008).
9. G. M. Gibson, S. D. Johnson, and M. J. Padgett, "Single-pixel imaging 12 years on: a review," *Opt. Express* **28**, 28190–28208 (2020).
10. M. P. Edgar, G. M. Gibson, and M. J. Padgett, "Principles and prospects for single-pixel imaging," *Nat. Photonics* **13**, 13–20 (2019).
11. N. Radwell, K. J. Mitchell, G. M. Gibson, M. P. Edgar, R. Bowman, and M. J. Padgett, "Single-pixel infrared and visible microscope," *Optica* **1**, 285–289 (2014).
12. M. P. Edgar, G. M. Gibson, R. W. Bowman, B. Sun, N. Radwell, K. J. Mitchell, S. S. Welsh, and M. J. Padgett, "Simultaneous real-time visible and infrared video with single-pixel detectors," *Sci. Reports* **5**, 10669 (2015).
13. M.-J. Sun, M. P. Edgar, G. M. Gibson, B. Sun, N. Radwell, R. Lamb, and M. J. Padgett, "Single-pixel three-dimensional imaging with time-based depth resolution," *Nat. Commun.* **7**, 12010 (2016).
14. S. D. Johnson, D. B. Phillips, Z. Ma, S. Ramachandran, and M. J. Padgett, "A light-in-flight single-pixel camera for use in the visible and short-wave infrared," *Opt. Express* **27**, 9829–9837 (2019).
15. Z. Zhang, X. Ma, and J. Zhong, "Single-pixel imaging by means of Fourier spectrum acquisition," *Nat. Commun.* **6**, 6225 (2015).
16. Z. Zhang, X. Wang, G. Zheng, and J. Zhong, "Fast Fourier single-pixel imaging via binary illumination," *Sci. Reports* **7**, 12029 (2017).
17. R. Liu, S. Zhao, P. Zhang, H. Gao, and F. Li, "Complex wavefront reconstruction with single-pixel detector," *Appl. Phys. Lett.* **114** (2019).
18. Y. Liu, P. Yu, X. Hu, Z. Wang, Y. Li, and L. Gong, "Single-pixel spiral phase contrast imaging," *Opt. Lett.* **45**, 4028–4031 (2020).
19. X. Hu, H. Zhang, Q. Zhao, P. Yu, Y. Li, and L. Gong, "Single-pixel phase imaging by fourier spectrum sampling," *Appl. Phys. Lett.* **114** (2019).
20. H. Ren, S. Zhao, and J. Gruska, "Edge detection based on single-pixel imaging," *Opt. Express* **26**, 5501–5511 (2018).
21. Z. Qiu, X. Guo, T. Lu, P. Qi, Z. Zhang, and J. Zhong, "Efficient Fourier single-pixel imaging with Gaussian random sampling," in *Photonics*, vol. 8 (MDPI, 2021), p. 319.
22. S. A. Goorden, J. Bertolotti, and A. P. Mosk, "Supapixel-based spatial amplitude and phase modulation using a digital micromirror device," *Opt. Express* **22**, 17999–18009 (2014).
23. Y.-X. Ren, Z.-X. Fang, L. Gong, K. Huang, Y. Chen, and R.-D. Lu, "Dynamic generation of Ince-Gaussian modes with a digital micromirror device," *J. Appl. Phys.* **117** (2015).
24. Y.-X. Ren, Z.-X. Fang, L. Gong, K. Huang, Y. Chen, and R.-D. Lu, "Digital generation and control of Hermite-Gaussian modes with an amplitude digital micromirror device," *J. Opt.* **17**, 125604 (2015).
25. E. Van Putten, I. M. Vellekoop, and A. Mosk, "Spatial amplitude and phase modulation using commercial twisted nematic LCDs," *Appl. Opt.* **47**, 2076–2081 (2008).
26. L. Waller, G. Situ, and J. W. Fleischer, "Phase-space measurement and coherence synthesis of optical beams," *Nat. Photonics* **6**, 474–479 (2012).
27. M. Woerdemann, C. Alpmann, M. Esseling, and C. Denz, "Advanced optical trapping by complex beam shaping," *Laser & Photonics Rev.* **7**, 839–854 (2013).
28. C. Maurer, A. Jesacher, S. Bernet, and M. Ritsch-Marte, "What spatial light modulators can do for optical microscopy," *Laser & Photonics Rev.* **5**, 81–101 (2011).
29. B. Bhaduri, C. Edwards, H. Pham, R. Zhou, T. H. Nguyen, L. L. Goddard, and G. Popescu, "Diffraction phase microscopy: principles and applications in materials and life sciences," *Adv. Opt. Photonics* **6**, 57–119 (2014).
30. A. B. Parthasarathy, K. K. Chu, T. N. Ford, and J. Mertz, "Quantitative phase imaging using a partitioned detection aperture," *Opt. Lett.* **37**, 4062–4064 (2012).
31. S. Turtaev, I. T. Leite, K. J. Mitchell, M. J. Padgett, D. B. Phillips, and T. Čižmár, "Comparison of nematic liquid-crystal and DMD based spatial light modulation in complex photonics," *Opt. Express* **25**, 29874–29884 (2017).
32. A. B. Ayoub and D. Psaltis, "High speed, complex wavefront shaping using the digital micro-mirror device," *Sci. Reports* **11**, 18837 (2021).